

Supplementary Material to the manuscript:

## The global SF<sub>6</sub> source inferred from long-term high precision atmospheric measurements and its comparison with emission inventories

Ingeborg Levin<sup>1</sup>, Tobias Naegler<sup>1</sup>, Renate Heinz<sup>1</sup>, Daniel Osusko<sup>1</sup>, Emilio Cuevas<sup>2</sup>, Andreas Engel<sup>3</sup>, Johann Ilmberger<sup>1</sup>, Ray L. Langenfelds<sup>4</sup>, Bruno Neininger<sup>5</sup>, Christoph v. Rohden<sup>1</sup>, L. Paul Steele<sup>4</sup>, Rolf Weller<sup>6</sup>, Douglas E. Worthy<sup>7</sup>, and Sergey A. Zimov<sup>8</sup>

- 1: Institut für Umweltphysik, Universität Heidelberg, INF 229, 69120 Heidelberg, Germany
- 2: Centro de Investigación Atmosférica de Izaña, Instituto Nacional de Meteorología (INM), C/ La Marina, 20, Planta 6, 38071 Santa Cruz de Tenerife, Spain
- 3: Institut für Atmosphäre und Umwelt, J.W. Goethe Universität Frankfurt, Altenhöferallee 1 D-60438 Frankfurt/Main, Germany
- 4: Centre for Australian Weather and Climate Research / CSIRO Marine and Atmospheric Research (CMAR), Private Bag No. 1, Aspendale, Victoria 3195, Australia
- 5: MetAir AG, Flugplatz, CH-8915 Hausen am Albis, Switzerland
- 6: Alfred Wegener Institut für Polar und Meeresforschung, Am Handelshafen 12, D-27570 Bremerhaven, Germany
- 7: Environment Canada, Climate Research Division / CCMR, 4905 Dufferin St., Toronto, ON M3H 5T4, Canada
- 8: North East Section of the Russian Academy of Sciences, P.O. Box 18, Cherskii, Republic of Sakha (Yakutia), Russia

### 1. The non-linearity of the Univ. of Heidelberg gas chromatographic system

Analysis of SF<sub>6</sub> mixing ratios is made by gas-chromatography with electron capture detector (GC-ECD) (Maiss et al., 1996). Maiss et al. used two different sample loops for the analysis of standard gas (93.7 ppt) and ambient air (0.6 to 3.5 ppt) samples with calibrated volumes of 1.006±0.002 cm<sup>3</sup> and 15.021±0.002 cm<sup>3</sup>, resp. This corresponds to about 3.8 fmols (1 fmol (femtomol) = 10<sup>-15</sup> mol) SF<sub>6</sub> detected in the case of the standard gas, and a range from 0.36 to 2.1 fmol in the case of ambient air samples. A linear response function of the ECD was assumed by Maiss et al. (1996) for the range of ambient mixing ratios measured at that time.

The analysis procedure has not been changed in recent years; however, the assumption of a strictly linear response curve of the ECD was abandoned in the present work, after a careful re-assessment of the non-linearity performed by Osusko (2007). Osusko used a number of accurately volume-calibrated sample loops in the range of 1.328±0.004 cm<sup>3</sup> to

26.792±0.007 cm<sup>3</sup> and a standard air sample of 5.757±0.003 ppt to determine the non-linearity of the ECD over a range of about 0.7 to 7 fmol SF<sub>6</sub>. Linearity-corrected mixing ratios are then calculated as follows: (1) The “raw” mixing ratio of a sample  $c_{\text{raw}}$  is first determined using an interpolated detector response based on the two nearest standard measurements bracketing the sample measurement. (2) Using actual temperature and pressure measurements as well as the volume of the sample loop (15.021 cm<sup>3</sup>) the actual sample amount  $n$  in amol (1 amol (attomol) = 10<sup>-18</sup> mol) is calculated. This value is then used to determine a correction factor  $A(n)$  according to Eq. 1 (Osusko, 2007):

$$A(n) = a_1 \cdot n + a_2 - \frac{a_2 \cdot a_3}{n + a_3} \quad (1)$$

with the coefficients  $a_1 = 1.03 \cdot 10^{-5} \text{ amol}^{-1}$ ,  $a_2 = -0.0474949$  and  $a_3 = 141.52704 \text{ amol}$ . A corrected mixing ratio  $c_{\text{corr}}$  is then calculated according to Eq. (2) using individually determined values of  $A(n)$

$$c_{\text{corr}} = c_{\text{raw}} \cdot \frac{1}{1 + A(n)} \quad (2)$$

Typical corrections for recent atmospheric samples (i.e. 4 to 6 ppt) range from +0.08 to +0.05 ppt. All measurements performed after December 2007 were corrected according to Eq. (1) and (2).

## 2. Corrections applied to data measured until December 2007 as well as to already published data (Maiss et al., 1996)

Besides referring their measurements to the working standard used as reference during all analyses (working standard 93, with a mixing ratio of 93.7 ppt injected to the standard sample loop of 1.006 cm<sup>3</sup>) Maiss et al. (1996) have used an additional set of air standards in the range of 1.6 to 3.2 ppt to correct individual measurement runs for an unknown blank contribution. In the following years, when atmospheric mixing ratios increased by almost a factor of two, we extended our set of ambient air standards to higher mixing ratios (up to 5.7 ppt) assuming a strictly linear response function, and applied respective blank corrections. Also, two new working standards had to be introduced, the gravimetrically prepared working standard 103 with a value of 103.25 ppt which was used from Aug. 22, 1998 to Aug. 12, 2003, and Standard N 114 used from Aug. 13, 2003 until August 2009. The mixing ratio of Standard N114 was determined via measurement against Standard 103. Its mixing ratio is 114.33 ppt.

In order to correct for non-linearity of the detector, the published data from Maiss et al. (1996) as well as the new data measured up to December 2007, we proceeded as follows:

For the two measurement periods where working standards 103 and N114 had been used, we re-calculated the concentration values of the air standards used for blank correction, and also selected a number of samples covering a large concentration range (i.e. samples that had been used for dilution experiments in other GC applications and also measured at the SF<sub>6</sub> GC) or where we analysed standard gases for other laboratories, and re-calculated corrected mixing ratios according to Eq. (1) and (2). Respective differences from the classical determination after Maiss et al. (1996) were then calculated and plotted against the classical uncorrected mixing ratio on the old Maiss scale (Figure A1).

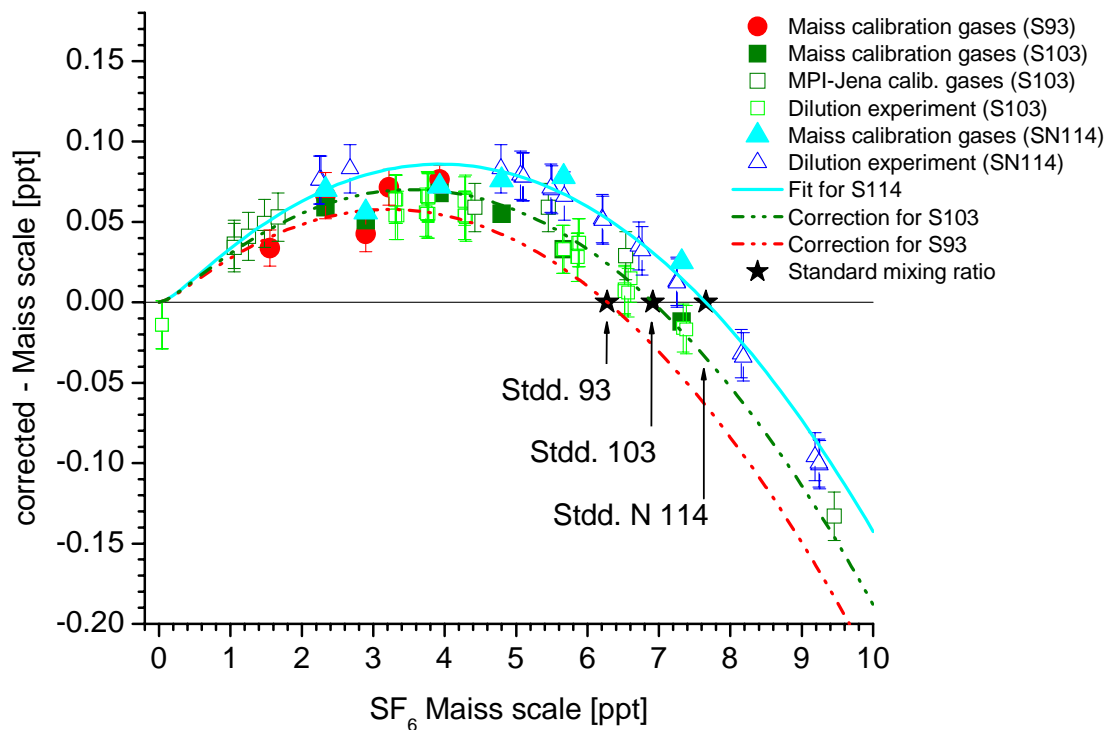


Figure A1:

Measured deviations of the Maiss scale from non-linearity. Maiss and subsequently used air standards are plotted as filled symbols while other samples analysed to independently check the non-linearity of the system (dilution experiments) are plotted with open symbols. Measurements against standard N114 are shown as triangles, against standard 103 as squares and against standard 93 as circles. The (virtual) standard mixing ratios corrected for sample loop volume are plotted as black stars. The light blue solid curve shows the correction function described by Eq. 1 and 2 (for standard N114). The dashed green and red lines show the correction functions used for the samples analysed against standards 103 and 93, which were obtained by adjusting the coefficients  $a_2$  and  $a_3$  in Eq. 1 for the respective standard mixing ratios. These correction curves excellently agree to the independent dilution samples as well as the air standards used since the beginning of the SF<sub>6</sub> program.

The differences between corrected and uncorrected mixing ratios follow the well-known shape typical for non-linearity of ECDs (compare e.g. Schmidt et al., 2001). The non-linearity correction should be zero at zero mixing ratios and also at the mixing ratio of the respective working standard used. As our working standards are measured in a smaller sample loop than our atmospheric samples the actual mixing ratios of the standards must be divided by the ratio of the sample loop volumes (14.931) to achieve the respective value. In the case of Standard 103 this corresponds to 6.915 ppt and for Standard N114 to a value of 7.657 ppt (the value for standard 93 is 6.275 ppt). The light blue solid curve in Figure A1 shows the correction function described by Eq. 1 and 2 (for standard N114). The dashed green and red lines show the correction functions used for the samples analysed against standards 103 and 93, which were obtained by adjusting the coefficients  $a_2$  and  $a_3$  in Eq. 1 for the respective standard mixing ratios. All samples measured relative to the respective standards have been corrected with these functions.

For all samples in the present atmospheric concentration range the non-linearity corrections are smaller than 0.08 ppt, with an absolute uncertainty of the correction smaller than 0.015 ppt. The total uncertainty of individual measurements is between 0.02 and 0.03 ppt.

Ongoing inter-comparison of air samples collected at the Cape Grim observatory shows a constant offset of about 0.1 ppt to AGAGE measurements and of about 0.07 ppt to NOAA/GMD (HD - AGAGE and HD - NOAA/GMD, respectively). These constant concentration offsets are due to independent calibration scale development of the different programs but has no influence on the growth rates and respective emission estimates.

### **3. Estimates of the atmospheric SF<sub>6</sub> inventory from tropospheric and stratospheric observations**

#### *3.1. Reconstruction of zonal mean surface SF<sub>6</sub> mixing ratios*

The reconstruction of the zonal mean surface SF<sub>6</sub> mixing ratios is based on the observed SF<sub>6</sub> records from the long-term background monitoring stations Alert (82°N), Izaña (28°N), Cape Grim (41°S) and Neumayer (71°S) as well as SF<sub>6</sub> data from regular aircraft sampling over Syktyvkar (61°N, only above 2500m). Flask and tank data from Alert, Cape Grim, and Neumayer, respectively, have been combined to obtain one single record for each of these stations. Subsequently, the data have been smoothed with a data fitting routine from Nakazawa et al. (1997), i.e. the seasonal cycle and outliers have been removed.

In a second step, we extrapolated the records from Alert, Syktyvkar, Izaña and Neumayer to the period where observations from Cape Grim are available (April 1978 - June 2009). The basic idea of this extrapolation is sketched here in the case of Alert: We used the

*simulated* SF<sub>6</sub> concentration gradient from the GRACE model (Levin et al., 2009)  $C_{\text{ALT}}^{\text{S}} - C_{\text{CGO}}^{\text{S}}$ , (superscript “S” for simulation) and added it to the observed (superscript “O”) SF<sub>6</sub> at Cape Grim ( $C_{\text{CGO}}^{\text{O}}$ ). To obtain a steady transition between the observed and reconstructed SF<sub>6</sub> at the beginning of the original Alert record, we adjusted the simulated gradient with a constant factor  $f_{\text{ALT}}$ . The reconstructed SF<sub>6</sub> concentration (superscript “R”) at Alert,  $C_{\text{ALT}}^{\text{R}}$ , thus was calculated as:

$$C_{\text{ALT}}^{\text{R}} = C_{\text{CGO}}^{\text{O}} + f_{\text{ALT}} \cdot (C_{\text{ALT}}^{\text{S}} - C_{\text{CGO}}^{\text{S}}) \quad (3)$$

In an identical manner, the extrapolation is performed for Syktyvkar, Izaña and Neumayer. Finally, the smoothed and extended station records have been interpolated to a regular latitude and time grid. Latitudinal interpolation is performed in sine of latitude space. Hereby, each smoothed/extended station record is assumed to represent the zonal mean SF<sub>6</sub> concentration at the latitude of the station. Additionally, SF<sub>6</sub> from Neumayer and Alert are assumed to represent also 90°S and 90°N, respectively. Furthermore, we duplicated the SF<sub>6</sub> record from Cape Grim at 15°S to imitate the shape of the observed zonal SF<sub>6</sub> concentration profile from the meridional transects over the Atlantic ocean (Maiss et al., 1996) where SF<sub>6</sub> concentrations south of 15°S are rather constant, whereas the increase from low mixing ratios in the southern hemisphere to high mixing ratios in the northern hemispheric starts approximately at 15°S.

### 3.2. *Reconstruction of representative vertical SF<sub>6</sub> profiles*

To avoid complications with different SF<sub>6</sub> scales, the reconstruction of representative vertical SF<sub>6</sub> concentration profiles is entirely based on stratospheric SF<sub>6</sub> profiles from samples measured in Heidelberg. Thus no SF<sub>6</sub> profiles from external publications have been taken into account.

To each stratospheric SF<sub>6</sub> profile, we added the tropospheric ground level SF<sub>6</sub> mixing ratio from the reconstructed surface level SF<sub>6</sub> mixing ratio field for the respective time and latitude of each stratospheric profile. The vertical SF<sub>6</sub> profiles then extend from the surface up to altitudes of 30-35km (depending on the profile). In doing so, we assume that SF<sub>6</sub> mixing ratio decreases linearly with pressure between the surface and the lowest altitude of each stratospheric profile. Subtraction of the surface SF<sub>6</sub> mixing ratio yields vertical SF<sub>6</sub> profiles relative to the surface level. These relative profiles – taken at different points in time – are now more comparable despite the increase in atmospheric SF<sub>6</sub> with time. The measured vertical SF<sub>6</sub> profiles (given on an altitude axis) are interpolated to a pressure axis using the altitude-pressure relationship from the U.S. Standard Atmosphere (COESA, 1976). For each of the three balloon stations (Kiruna, Aire sur l’Adour, Teresina), we then calculated the average relative vertical SF<sub>6</sub> mixing ratio profile.

From a simple box-model point of view, the vertical profile of a tracer with sources at the surface and no sinks in the atmosphere should scale nearly linearly with the surface source. From the temporal derivative of the fit curve through the tropospheric SF<sub>6</sub>

observations we obtain a first-order estimate of the temporal behaviour of the global SF<sub>6</sub> source, which increased nearly linearly between 1978 (the start of our observations) and 1995. Between 1995 and the early 2000s, the global SF<sub>6</sub> source decreased slightly, before it started to increase again. It is therefore reasonable to assume that vertical SF<sub>6</sub> profiles increased nearly linearly until the early 1990s and are more or less constant from this time on. We thus assume that the averaged relative gradients for each profile station (averaged over all post-1990 profiles) well represent the relative vertical gradient above these stations (i.e. at the respective latitude) in this period (see Figure A2).

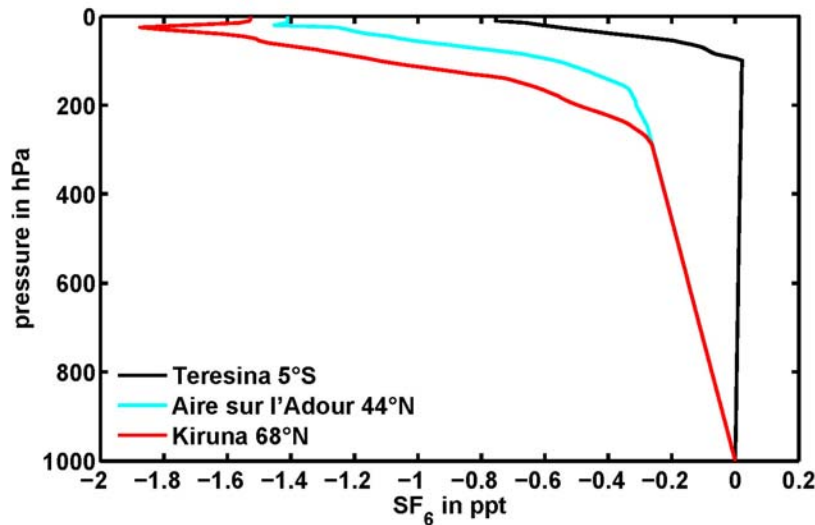


Figure A2:  
Average stratospheric SF<sub>6</sub> profiles relative to the bottom-near troposphere for Teresina, Aire sur l'Adour and Kiruna.

For pre-1990, we obtained relative vertical gradients for each station (Kiruna, Aire sur l'Adour, Teresina) by scaling the observed average relative profile with the reconstructed surface SF<sub>6</sub> mixing ratio (at the given latitude) relative to the 1990 surface mixing ratio. Thus we obtain a time series of relative vertical SF<sub>6</sub> profiles between 1978 and 2009 for each of the three profile stations.

Tests with our GRACE model (Levin et al., 2010) have shown that the vertical SF<sub>6</sub> gradient in the southern extra-tropics (where no profile data are available) is well approximated by scaling the simulated vertical SF<sub>6</sub> gradient in northern mid-latitudes with a factor 0.56. We thus assumed that the reconstructed, observation-based average relative vertical profile in Kiruna well represents the relative vertical profile in northern polar latitudes (60°N-90°N), whereas Aire sur l'Adour represents northern mid-latitudes (30°N-60°N) and Teresina the tropics (30°S-30°N). Furthermore, we assumed that the relative profile from Aire sur l'Adour, scaled with a factor 0.56, represents the relative vertical SF<sub>6</sub> profile in the southern extra-tropics (90°S-30°S). We thus obtain a time

series of estimates of vertical SF<sub>6</sub> profiles (relative to surface mixing ratios) from 90°S to 90°N and from 1978 - 2009.

### *3.3. Estimate of the global atmospheric SF<sub>6</sub> inventory, annual source strength and uncertainties*

Combining the reconstructed surface SF<sub>6</sub> concentrations with the reconstructed relative vertical SF<sub>6</sub> profiles, we obtain a reconstruction of the global SF<sub>6</sub> concentration on a latitude - pressure grid between April 1978 and June 2009. Averaging over the entire atmosphere (i.e. from 1000hPa to 10hPa, the lowest pressure level), we obtain the global average SF<sub>6</sub> concentration for the period in question, from which the global SF<sub>6</sub> inventory can be calculated. Finally, the global SF<sub>6</sub> source is the temporal derivative of the global atmospheric SF<sub>6</sub> inventory (Table 2 of the main manuscript).

A number of uncertainties affect the reconstructed SF<sub>6</sub> field, our estimate of the global SF<sub>6</sub> inventory and - to a weaker extent - the global SF<sub>6</sub> source: First, the uncertainty of the individual tropospheric SF<sub>6</sub> measurement is of the order 0.02 ppt. The fitting procedure is not expected to add significant uncertainty (at least on an annual mean basis). The extension of the observed SF<sub>6</sub> records from Alert, Izaña, and Neumayer Station is based on the assumption that the relative temporal change of SF<sub>6</sub> concentration differences between these stations and Cape Grim is well reproduced by the GRACE model. Spatial SF<sub>6</sub> gradients are predominantly controlled by the spatial pattern of SF<sub>6</sub> emissions. Thus, the change in the gradients is controlled by changing emissions. As all estimates of global SF<sub>6</sub> emissions in the 1980s and early 1990s (Maiss and Brenninkmeijer, 1998; Olivier and Berdowski, 2001; EDGAR, 2009) show a similar, nearly linear increasing trend also used in the GRACE simulations, it is reasonable to assume that the relative temporal change of SF<sub>6</sub> gradients is well captured by GRACE. However, due to uncertainties in the atmospheric transport, the absolute value of the gradients might be over- or underestimated by GRACE. This problem becomes evident in particular for Izaña, where observed SF<sub>6</sub> mixing ratios (and thus concentration differences to neighbouring stations) are not well matched by GRACE. However, as mentioned above, we adjusted the simulated gradients in a way to guarantee a steady transition of reconstructed and observed station records to overcome shortcomings of the atmospheric transport in GRACE. Thus, uncertainties in the extended SF<sub>6</sub> records are of similar order of magnitude as inter-annual variability in the original records caused by inter-annual variability of atmospheric transport, which is not taken into account in GRACE. From the available atmospheric SF<sub>6</sub> records, this variability is estimated not to exceed 0.03 ppt.

SF<sub>6</sub> concentration variability in the Southern Hemisphere south of 15°S is on the order of ca. ±0.05 ppt (Maiss et al., 1996; Geller et al., 1997). This value can be taken as an upper limit of the uncertainty of our reconstruction of zonal mean SF<sub>6</sub> mixing ratio south of 15°S. Similarly, in the Northern Hemisphere north of Izaña (28°N), where most of the SF<sub>6</sub> sources are located, the variability is on the order of ca. ±0.1 ppt (Maiss et al., 1996; Geller et al., 1997), which gives an estimate of the uncertainty of our reconstruction for the northern extra-tropics. Both Maiss et al. (1996) and Geller et al. (1997) show a nearly

linear decrease of SF<sub>6</sub> concentrations across the tropics (30°N-15°S). We thus can assume that uncertainties in our reconstruction of tropical SF<sub>6</sub> concentrations are small, probably on the order of 0.05 ppt. As a consequence, the overall uncertainty of our reconstructed zonal mean surface SF<sub>6</sub> concentrations is expected to be on the order of 0.06-0.11 ppt, with higher uncertainty in the Northern Hemisphere, in particular in the 1980s and early 1990s (when northern hemispheric mixing ratios are entirely reconstructed).

The uncertainty of the average stratospheric profiles (relative to surface mixing ratios) can be addressed by the standard deviation of the profiles at each station. For the extra-tropical stations Kiruna and Aire sur l'Adour, this is on the order of 0.2-0.3 ppt above 300 hPa. For the two measured profiles at the tropical station Teresina, the standard deviation of the vertical SF<sub>6</sub> profiles above 300 hPa is less than 0.1 ppt. In addition to differences between observed profiles, non-quantifiable uncertainties in the pressure-altitude relationship used in our approach might contribute to biases in the reconstructed global mean SF<sub>6</sub> mixing ratios and inventory time series. In summary, we thus assume that the stratospheric SF<sub>6</sub> mixing ratios relative to surface are well reconstructed within 0.1-0.3 ppt.

In our approach, we implicitly assume that SF<sub>6</sub> concentration increases linearly from the lowest profile measurements to the surface. Aircraft-based SF<sub>6</sub> profile measurements from Syktyvkar (62°N), Cherskii (69°N), and Cape Grim (41°S) show an SF<sub>6</sub> concentration variability on the order of 0.04-0.06 ppt below 3000m (below 7600m at Cape Grim). However, aircraft data show no clear decrease in SF<sub>6</sub> concentration within the Planetary Boundary Layer (PBL), except for Cape Grim, where SF<sub>6</sub> concentrations below 1000m are *lower* than concentrations above. However, in general, it seems to be appropriate that SF<sub>6</sub> concentration variability within the background troposphere is - on average - less than 0.05ppt.

If we combine these uncertainty estimates, the absolute uncertainty of the global (tropospheric and stratospheric) annual mean SF<sub>6</sub> mixing ratio is of the order 0.12-0.14 ppt. However, most of the factors contributing to the uncertainties discussed above are probably constant in time or change only slightly with changing SF<sub>6</sub> emissions and the resulting change in horizontal and vertical SF<sub>6</sub> gradients. Thus, the main factor of uncertainty of our SF<sub>6</sub> source estimate appears to be the variability of the observed SF<sub>6</sub> growth rate among the different stations: In Figure 1 of the main manuscript we show smoothed growth rate curves determined for all our tropospheric sites. The standard deviation of 10-day growth rate values of all curves for the period of 1991 to 2007 ranges from 0.002 to 0.02 ppt a<sup>-1</sup>, with a mean value of 0.012 ppt a<sup>-1</sup>. If we take this value as the mean uncertainty of annual growth rates, this corresponds to an error of ±6%, also for the source estimate for the time period in question.

#### 3.4. Comparison with other top-down estimates of the global SF<sub>6</sub> source

Figure A3 compares estimates of the global SF<sub>6</sub> source from this study with other top-down estimates of this quantity. Within 2σ of our estimated uncertainty (of 1σ = ±6%),



we agree well with estimates from Geller et al. (1997), Maiss and Brenninkmeijer (1998), de Jager et al. (2005) and Forster et al. (2007). However, while our estimate indicates that global SF<sub>6</sub> emissions continue to increase after the minimum in 1998, the IPCC data from Forster et al. (2007) suggest a strong decrease of the SF<sub>6</sub> source between 2003 and 2005 which can not be seen in our data. Furthermore, in contrast to the Heidelberg data, NOAA/CMDL flask data (de Jager et al., 2005) suggest a drop in SF<sub>6</sub> emissions of ca. 20% in 1998 and 1999 (relative to 1997), followed by an increase of the SF<sub>6</sub> source of similar magnitude from 2000 on. A corresponding variability of the SF<sub>6</sub> growth rate can not be seen at any of the stations of the Heidelberg network in the respective period (compare Figure 1 of the main manuscript). From this we conclude that SF<sub>6</sub> emissions based on NOAA/CMDL data (de Jager et al., 2005; Forster et al., 2007) possibly overestimate the inter-annual variability of the SF<sub>6</sub> source (note, however, that no error estimates are given in these studies).

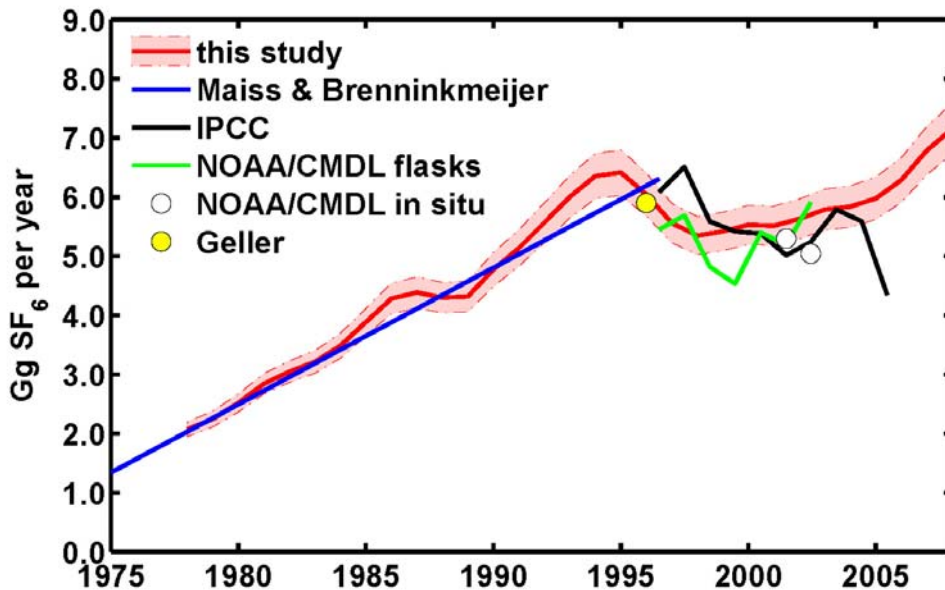


Figure A3:

Comparison of top-down estimates of the global SF<sub>6</sub> source. References: red line and shaded area: best estimate and 1 $\sigma$  uncertainty range from this study; light blue line: Maiss and Brenninkmeijer (1998); black line: Forster et al. (2007); green line and white circles: de Jager (2005), yellow circle: Geller et al. (1997).

#### 4. Bottom-up SF<sub>6</sub> emission estimates

##### 4.1 *Compilation of SF<sub>6</sub> emission estimates*

Note that the SF<sub>6</sub> inventory presented here is the annual mean, whereas the SF<sub>6</sub> source is calculated as the change of the global atmospheric SF<sub>6</sub> inventory between January 1<sup>st</sup> of each year and January 1<sup>st</sup> of the following year. Note further that UNFCCC reports SF<sub>6</sub>

emissions in units of CO<sub>2</sub>-equivalent. To calculate SF<sub>6</sub> emissions in Gg, we used a Global Warming Potential for SF<sub>6</sub> (100 years time horizon) of 23900, as used in UNFCCC reporting by Annex I countries, which is higher than the value adopted by IPCC (Forster et al., 2007) of 22800.

#### 4.2. *Correction applied to the SF<sub>6</sub> emission values reported by Japan to UNFCCC*

Japan reported emissions of 1.9 Gg SF<sub>6</sub> for 1994, but only 0.7 Gg SF<sub>6</sub> for the following year. This apparent decrease in Japanese SF<sub>6</sub> emissions is due to changed methodology estimating SF<sub>6</sub> emissions between 1994 and 1995: The old methodology applied until 1994 probably grossly overestimates the emissions, whereas the new method (applied from 1995 onwards) is expected to provide more realistic estimates of the Japanese SF<sub>6</sub> source (Jigme (UNFCCC), personal communication 2008). Independent estimates of Japanese SF<sub>6</sub> emissions from gas insulated electrical equipment in Japan (Yasutake and Meguro, 2002) indicate roughly constant SF<sub>6</sub> emissions in the early-to-mid-1990s, before SF<sub>6</sub> emissions actually were reduced from the mid-1990s on. To correct the Japanese pre-1995 emissions (and thus the total Annex I SF<sub>6</sub> emissions in this period), we therefore assumed that the Japanese SF<sub>6</sub> emissions in 1990-1994 are identical with the emissions in 1995, the first year when the new methodology was applied.

#### 4.3. *Reconstruction of the meridional distribution of the UNFCCC-based emission scenario*

Annex I country emissions are individually reported to UNFCCC (UNFCCC, 2009), so that a first-order estimate of the SF<sub>6</sub> source distribution from Annex I countries can be derived from the individually reported SF<sub>6</sub> emissions and the geographical location of each Annex I country. For Non-Annex I countries no reliable SF<sub>6</sub> emissions estimates on the country level are available from UNFCCC. Only the *total* Non-Annex I emissions can be estimated as the difference between observation-based inferred *global* emissions and Annex I (UNFCCC-reported) emissions (see main manuscript). However, following Denning et al. (1999), we can roughly estimate the spatial distribution of SF<sub>6</sub> emissions from Non-Annex I countries, if we assume that the geographical distribution of non-Annex I SF<sub>6</sub> emissions is similar to the distribution of Non-Annex I electricity production (BP, 2009). In this way, we obtain an UNFCCC-based estimate of the *total* spatial distribution of SF<sub>6</sub> sources on the globe (compare Supplementary Fig. 4b). Note that this approach does *not* assume similar ratios of SF<sub>6</sub> emissions per unit electricity produced by Annex I and non-Annex I countries. However, we do assume that this emission ratio varies with time and is the same in all non-Annex I countries.

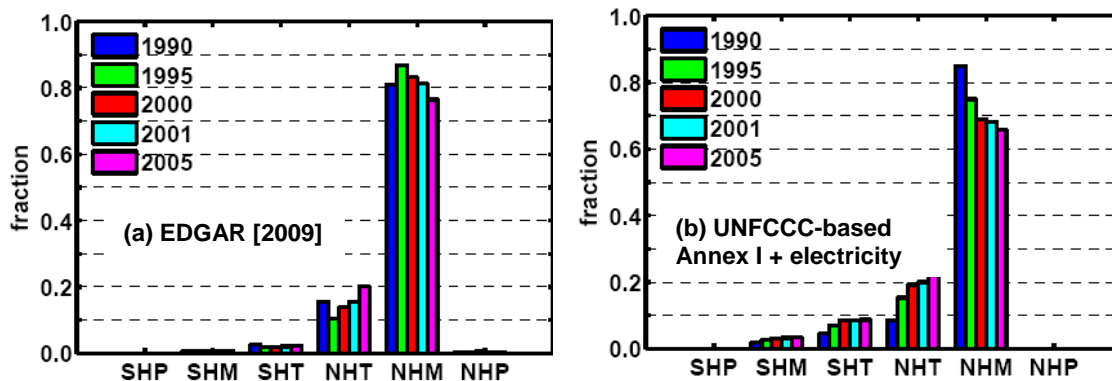


Figure A4:

Fraction of SF<sub>6</sub> emissions averaged over 30° zonal bands for 1990, 1995, 2000, 2001 and 2005. SHP: 90°S to 60°S, SHM: 60°S to 30°S, SHT: 30°S to Equator, NHT: Equator to 30°N, NHM: 30°N to 60°N, NHP: 60°N to 90°N. (a) SF<sub>6</sub> emission distribution based on EDGAR (2009). (b) SF<sub>6</sub> emission distribution based on UNFCCC reported SF<sub>6</sub> emissions.

## References Supplementary Material

BP, British Petroleum Statistical Review of World Energy: available online at <http://www.bp.com/statisticalreview>, 2009.

COESA, Committee on Extension to the Standard Atmosphere: U.S. Standard Atmosphere: U.S. Government Printing Office, Washington D.C., U.S.A., 1976

de Jager, D., Safeguarding the Ozone Layer and the Global Climate System: Issues Related to Hydrofluorocarbon and Perfluorocarbons, *IPCC/TEAP Special Report*, UNFCCC, Bonn, Germany, 2005.

Denning, A.S., Holzer, M., Gurney, K.R., Heimann, M., Law, R.M., Rayner, P.J., Fung, I.Y., Fan, S.-M., Taguchi, S., Friedlingstein, P., Balkanski, Y., Maiss, M. and Levin, I.: Three-dimensional transport and concentration of SF<sub>6</sub>: A model intercomparison study (TransCom 2), *Tellus*, 51B, 266-297, 1999.

EDGAR, Emission Database for Global Atmospheric Research (EDGAR): European Commission, Joint Research Centre (JRC)/Netherlands Environmental Assessment Agency (PBL), release version 4.0. <http://edgar.jrc.ec.europa.eu>, 2009.

Forster, P., Ramaswamy, V., Artaxo, P., Berntsen, T., Betts, R., Fahey, D.W., Haywood, J., Lean, J., Lowe, D.C., Myhre, G., Nganga, J., Prinn, R., Raga, G., Schulz, M. and Van Dorland, R.: Changes in Atmospheric Constituents and in Radiative Forcing. In: *Climate Change 2007: The Physical Science Basis. Contribution of Working Group I to the Fourth Assessment Report of the Intergovernmental Panel on Climate Change* [Solomon, S., D. Qin, M. Manning, Z. Chen, M. Marquis, K.B. Averyt, M. Tignor and H.L. Miller (eds.)]. Cambridge University Press, Cambridge, United Kingdom and New York, NY, USA, 2007.

Geller, L. S., Elkins, J.W., Lobert, J.M., Clark, A.D., Hurst, D.F, Butler, J.H., and Myers, R.C.: Tropospheric SF<sub>6</sub>: Observed latitudinal distribution and trends, derived

- emissions and interhemispheric exchange time, *Geophys. Res. Lett.*, 24(6), 675-678, 1997.
- Levin, I., Naegler, T., Kromer, B., Diehl, M., Francey, R.J., Gomez-Pelaez, A.J., Steele, L.P., Wagenbach, D., Weller, R., and Worthy, D.E.: Observations and modelling of the global distribution and long-term trend of atmospheric  $^{14}\text{CO}_2$ , *Tellus 62B*, 26-46, doi: 10.1111/j.1600-0889.2009.00446.x, 2010.
- Maiss, M. and Brenninkmeijer, C.A.M.: Atmospheric  $\text{SF}_6$ : Trends, sources, and prospects, *Environ. Sci. Technol.*, 32, 3077-3086, 1998.
- Maiss, M., Steele, L.P., Francey, R.J., Fraser, P.J., Langenfelds, R.L., Trivett, N.B.A. and Levin, I.: Sulfur hexafluoride – a powerful new atmospheric tracer, *Atmos. Environ.*, 30, 1621-1629, 1996.
- Nakazawa, T., Ishizawa, M., Higuchi, K. and Trivett, N.B.A.: Two curve fitting methods applied to  $\text{CO}_2$  flask data, *Environmetrics*, 8, 197-218, 1997.
- Olivier, J.G.J. and Berdowski, J.J.M.: Global emissions sources and sinks. In: Berdowski, J., Guicherit, R. and B.J. Heij (eds.) *The Climate System*, 33-78, A.A. Balkema Publishers/Swets & Zeitlinger Publishers, Lisse, The Netherlands. ISBN 90 5809 255 0, 2001.
- Osusko, D.: Kalibrierung eines Gaschromatographen zur Messung von Schwefelhexafluorid. *Thesis, Institut für Umweltp Physik*, University of Heidelberg, 2007.
- Schmidt, M., Glatzel-Mattheier, H., Sartorius, H., Worthy, D.E. and Levin, I.: Western European  $\text{N}_2\text{O}$  emissions – a top down approach based on atmospheric observations, *J. Geophys. Res.*, 106, D6, 5507-5516, 2001.
- UNFCCC. National greenhouse gas inventory data for the period 1995-2006, Secretariat of the United Nation Framework Convention on Climate Change, Bonn, Germany, data available online at [http://unfccc.int/ghg\\_data/items/4133.php](http://unfccc.int/ghg_data/items/4133.php), 2009.
- Yasutake, H. and Meguro, M.  $\text{SF}_6$  emission reduction from gas insulated electrical equipment in Japan. *Proceedings of the 2<sup>nd</sup> International Conference on  $\text{SF}_6$  and the Environment*, San Diego, USA, 2002.